Magnetic toroidal dipole resonances for efficient THz generation in dielectric metasurfaces

Davide Rocco, Olga Sergaeva, Luca Carletti, Andrea Tognazzi, Paolo Franceschini, Alfonso Carmelo Cino, Andrea Locatelli, and Costantino De Angelis

***Abstract*—Nonlinear dielectric metasurfaces represent a rapidly advancing family of optical devices characterized by high nonlinear conversion efficiency with an ultrathin form factor. Here, we report on terahertz (THz) emission through difference-frequency generation (DFG) in an Aluminum Gallium Arsenide (AlGaAs) metasurface supporting magnetic toroidal dipolar resonances at the two pump wavelengths, which nonlinearly interact with each other. The simultaneous excitation of these high-Q resonances, together with the dispersive behavior of the nonlinear susceptibility, enables an exceptionally strong DFG response. Conversion efficiencies around 8 THz exceed those of an unstructured AlGaAs slab of the same thickness by over nine orders of magnitude. These results highlight the potential of DFG metasurfaces as compact and highly efficient platforms for THz generation.**

***Index Terms*—Metasurfaces, Terahertz radiation, toroidal magnetic fields, dielectric resonator antennas, nonlinear optics.**

I. INTRODUCTION

ALL-dielectric metasystems have emerged as highly adaptable platforms for controlling electromagnetic wave propagation with exceptional precision [1], [2], [3], [4]. Unlike metallic nanostructures that rely on plasmonic resonances, dielectric architectures sustain both electric and magnetic Mie-type multipolar modes, enabling extensive control over the spatial distribution of near- and far-field responses [5], [6]. Moreover, their intrinsically low optical losses compared to noble metals lead to markedly enhanced performance in photonic and optoelectronic devices based on dielectric metasurfaces [7], [8]. These structures are also inherently compatible with standard complementary metal–oxide–semiconductor (CMOS) fabrication technologies [9], [10], [11].

Concurrently, the generation and detection of terahertz (THz) electromagnetic waves (1–10 THz) are attracting growing attention due to their relevance in applications with strong societal impact, including medical imaging, security screening, and ultra-fast wireless communications [12], [13], [14], [15]. Bringing THz technologies from laboratory research to practical implementation requires sources and detectors that are efficient, compact, and cost-effective. In this context, DFG in all-dielectric nanoantennas is particularly appealing, as it enables the down-conversion of information signals into the THz range, starting from the telecommunication band where a wide array of mature devices is already available [16], [17]. Therefore, nanoscale engineered structures offer opportunities for highly miniaturized THz systems. In particular, it has recently been demonstrated that THz via DFG from dielectric nanocylinders (made of AlGaAs) is approximately seven times more efficient than its metallic counterpart, owing to the ability of the electromagnetic field to be confined within the dielectric material [16]. This enables volume, not merely surface, nonlinear contributions. The aforementioned theoretical prediction has been confirmed experimentally, where THz emission via DFG is observed from a dielectric metasurface [18]. Nevertheless, the overall THz generation efficiency remained relatively low, as the resonances employed at the pump frequencies exhibited limited Q-factors. Notably, resonant modes with long photon lifetimes at the pumps enhance the local field intensity, which directly boosts the nonlinear DFG efficiency. It is therefore of particular interest to design a device supporting high-Q resonances at the fundamental frequencies. In this context, toroidal dipole (TD) resonances have attracted growing interest for their relevance in both fundamental studies and applied photonics [19], [20], [21]. Although they produce far-field radiation patterns similar to those of electric (ED) and magnetic dipoles (MD), their near-field configurations are uniquely distinct [22], [23]. More recently, TD resonances exhibiting high-Q factors have drawn considerable attention owing to their ability to markedly enhance light–matter interactions [24], [25], [26], [27], [28]. Most reported TD modes correspond to electric toroidal dipoles (ETDs), where the electric field is concentrated in air gaps or holes [29], [30]. In contrast, magnetic toroidal dipole (MTD) modes have been demonstrated only in a few studies [31], [32], [33], [34], [35], [36]. Unlike ETDs, MTDs provide superior confinement of the electric field within the dielectric medium, making them promising candidates for semiconductor metasurfaces designed for lasing and nonlinear harmonic generation. For instance, in [33], the excitation of a MTD mode in a silicon nanoblock metasurface with a high Q-factor is theoretically and experimentally demonstrated. Subsequently, this concept has been revisited and applied to various contexts, including ultrasensitive sensing applications [34], nonlinear chiroptical

This work was supported in part by the European Union–Next Generation EU, Mission 4 Component 1-PRIN 2022 project GRACE6G (2022H7RR4F) CUP D53D23001250001. *(Corresponding author: Davide Rocco).*

Davide Rocco, Luca Carletti, Paolo Franceschini, Andrea Locatelli and Costantino De Angelis are with the Department of Information Engineering, University of Brescia, via Branze 38, 25123 Brescia, Italy, also with the National Institute of Optics, Consiglio Nazionale delle Ricerche, via Branze 45, 25123 Brescia, Italy (e-mail: davide.rocco@unibs.it; luca.carletti@unibs.it; paolo.franceschini@unibs.it; andrea.locatelli@unibs.it; costantino.deangelis@unibs.it). Olga Sergaeva is with the Department of Information Engineering, University of Brescia, via Branze 38, 25123 Brescia, Italy (e-mail: olga.sergaeva@unibs.it). Andrea Tognazzi and Alfonso Carmelo Cino are with the Department of Engineering, University of Palermo, Viale Delle Scienze, 90128 Palermo, Italy (e-mail: andrea.tognazzi@unipa.it; alfonsocarmelo.cino@unipa.it).

Manuscript received April 19, 2021; revised August 16, 2021.

response [36] and boosted second-harmonic generation in lithium niobate metasurfaces [35].

In this work, we investigate efficient THz emission via DFG by exploiting two high-Q magnetic toroidal dipole resonances at the pump frequencies supported by an AlGaAs metasurface. The interplay between the two high-Q resonances and the dispersive $\chi^{(2)}$ response of AlGaAs enables highly efficient THz generation (up to 0.05 W^{-1}), exceeding by nine orders of magnitude that of an unstructured AlGaAs slab of the same thickness. This approach fits within the broader and rapidly emerging paradigm of dual- or multi-resonant enhancement of nonlinear parametric processes in dielectric metasurfaces, which has been successfully explored in related contexts such as sum-frequency generation and four-wave mixing using quasi-bound states in the continuum or multi-resonant designs [37], [38], [39], [40], [41], [42], [43], [44]. Beyond this general framework, our results demonstrate that a semicondutor-based metasurface with a relatively simple design, compatible with current fabrication standards, can efficiently generate THz radiation by simultaneously exploiting high-Q magnetic toroidal resonances occurring at the pump frequencies and the peaks amplitude of the dielectric $\chi^{(2)}$ susceptibility. To the best of our knowledge, this investigation provides the first theoretical demonstration of terahertz DFG enabled by the simultaneous excitation of two high-Q magnetic toroidal dipole resonances, thereby extending multi-resonant nonlinear metasurface concepts to the THz DFG regime. Overall, this work contributes to advancing the design principles of nonlinear metasurfaces for efficient THz generation.

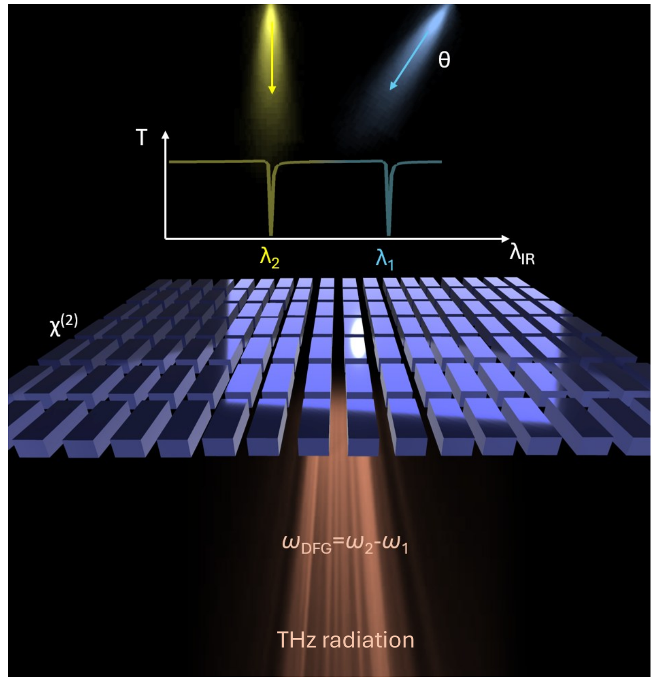

Fig. 1. Sketch of the proposed device. The AlGaAs metasurface is illuminated by two pump beams: one at normal incidence with wavelength λ_2, and the other at wavelength λ_1 incident at an angle θ. The metasurface is engineered to support high-Q magnetic toroidal dipolar resonances at both λ_1 and λ_2, thereby enhancing the DFG emission at $\omega_{\mathrm{DFG}} = \omega_2 - \omega_1$.

II. Results and discussion

The need for high-Q resonance is addressed here by leveraging MTD resonances, thereby enabling the realization of a doubly-resonant dielectric meatasurface as conceptually reported in Fig.1.

To implement this concept, we design a dielectric metasurface whose unit cell is engineered to sustain the required toroidal magnetic resonances. All the simulations are performed using the finite element method (FEM) implemented in COMSOL Multiphysics. The metasurface consists of an array of AlGaAs elements arranged on a silicon dioxide substrate. The unit cell has a square lattice with a period of $P = 940$ nm and includes two dielectric nano-blocks with a length of $s = 650$ nm, a width of $w = 210$ nm, and a height of 340 nm, as reported in Fig 2(a). Each block is displaced from the center of the cell by a distance of $P/4 + L$, where L represents the asymmetry parameter. The geometrical parameters are adopted from previously reported designs to ensure the excitation of the toroidal resonance in the near infrared (NIR) region [33]. Indeed, Fig. 2(a) shows the Cartesian decomposition in the NIR spectral domain, clearly highlighting that the dominant contribution arises from the magnetic toroidal dipole, which is excited at the wavelength $\lambda_2 = 1452.56$ nm when $L = 10$ nm under plane-wave illumination polarized along the x-direction. The multipole decomposition is computed as reported in [33]. In Fig. 2(b), the electric and magnetic field distributions are reported, showing the characteristic field patterns associated with the MTD mode, together with a local electric field enhancement inside the nanoblocks reaching about 40 times the incident field amplitude. This resonance exhibits a very high Q-factor ($\approx 7 \times 10^3$), as can also be observed from the transmission dip (blue curve) reported in Fig. 2(c) as a function of wavelength. As similarly observed in [33], the dip in transmission broadens as L increases. For very small L values (e.g., $L = 2$ nm), the resonance peak in transmission becomes increasingly narrow, and the resonance eventually disappears when $L = 0$. This indicates that this mode can be effectively excited by varying the distance between the nanoblocks (i.e. for $L \neq 0$). Such behavior identifies the mode as a quasi-bound state in the continuum (qBIC), whose high Q-factor depends on the inter-block spacing [45]. The inset in Fig. 2(c) further illustrates how the Q-factor varies with increasing L, confirming the dependence of the resonance sharpness on the inter-block spacing.

Beyond its sensitivity to the structural parameter L, the MTD resonance remains efficiently excitable over a finite angular range. In this regard, Fig. 2(d) shows the dispersion of the MTD mode as a function of the incidence angle of the impinging radiation (θ). A p-polarized illumination with a maximum angle of $\theta = 8^\circ$ is considered to avoid diffractive orders. As θ increases, the spectral position of the transmission dip red-shifts from ≈ 1452 nm to ≈ 1516 nm, while preserving the characteristic MTD nature of the resonance. This angular-dependent spectral tunability of the MTD resonance can be exploited to efficiently generate a tunable THz signal through the nonlinear DFG process. In other words, the main advantage

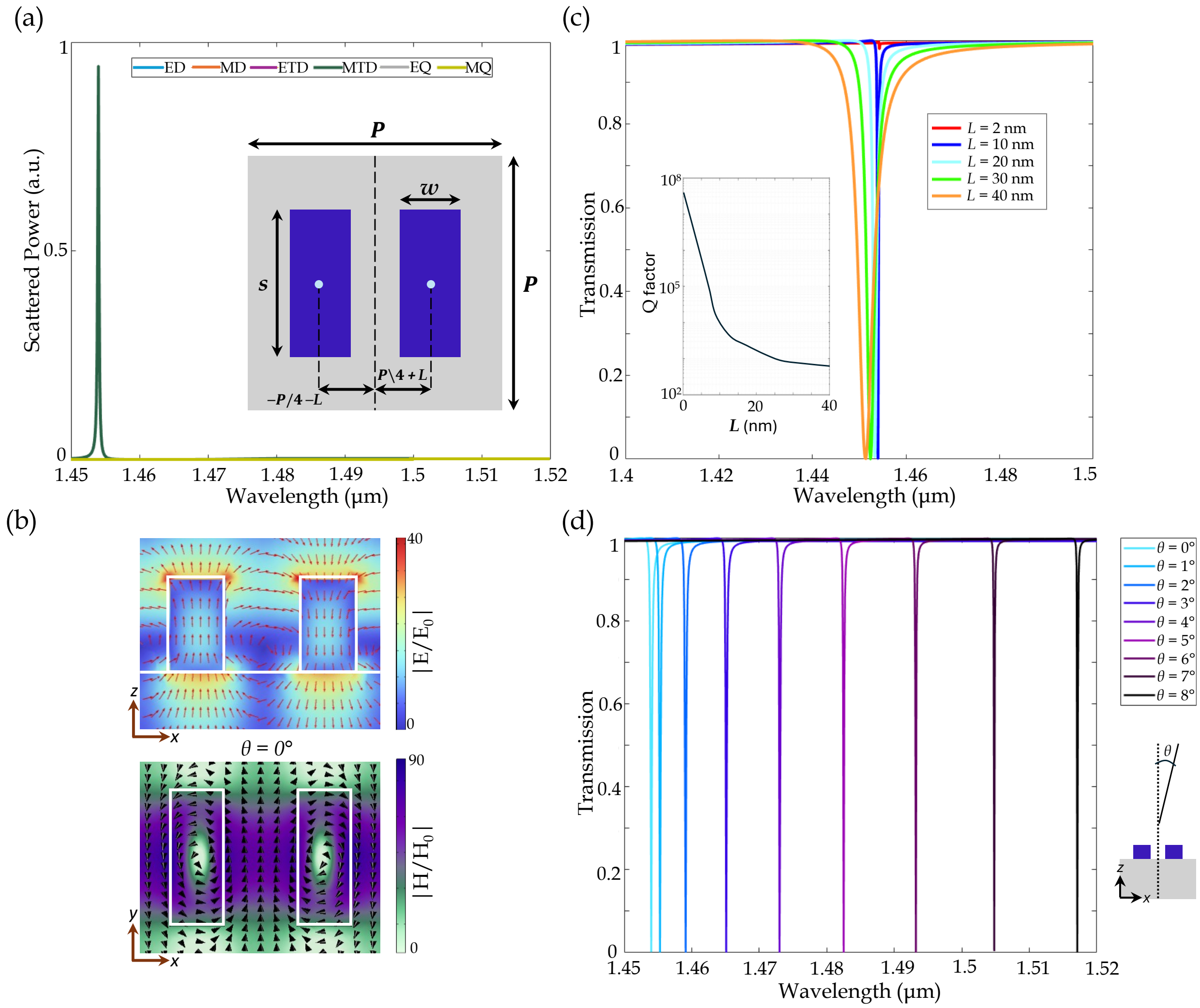

Fig. 2. (a) Cartesian multipolar decomposition showing the contributions from the electric dipole (ED), magnetic dipole (MD), electric toroidal dipole (ETD), magnetic toroidal dipole (MTD), electric quadrupole (EQ), and magnetic quadrupole (MQ). The inset illustrates the geometrical parameters of the unit cell: the bluish regions correspond to the AlGaAs nanoblocks, while the gray region represents the SiO_2 substrate. (b) Electric (top) and magnetic (bottom) field distributions under normal incidence for $L = 10$ nm at the MTD resonance wavelength $\lambda_2 = 1452.56$ nm. E_0 and H_0 represent the incident electric and magnetic field amplitude, respectively. (c) Transmission spectra as a function of wavelength for different values of L. The inset shows the reduction of the Q-factor as the asymmetry parameter L increases. (d) Transmission spectra as a function of wavelength for increasing incidence angles θ under p-polarized illumination.

of MTD resonances for THz generation lies in their high-Q nature and pronounced angular dispersion, which allow the same qBIC mode to be efficiently excited at different frequencies by varying the incidence angle. This provides strong and selective field enhancement for both pump waves, enabling efficient nonlinear mixing. By comparison, low-Q MD or ED resonances have broad spectral linewidths and weak angular sensitivity, so the same resonance is overlapped with multiple pump frequencies, limiting nonlinear efficiency. Anapole modes, on the other hand, are constrained by a delicate destructive-interference condition, making intrinsically difficult to achieve doubly resonant excitation at two independent pump frequencies. Specifically, we now consider the metasurface excited by two optical sources: one fixed around λ_2 with normal incidence, and the other impinging at an oblique angle with variable wavelength λ_1 and incidence angle θ. The DFG problem is addressed following the same numerical procedure reported in [16]. Namely, the implementation involves three computational stages: the first two solve the linear response at the pump wavelengths using the scattering field formulation, and the resulting fields are employed to compute the nonlinear sources. The third step consists of a full-field simulation at the THz frequency, where the nonlinear currents sources $J_i(\omega_{DFG})$ that drive the emitted THz field are expressed as: $J_i(\omega_{DFG}) = -i\omega_{DFG}\epsilon_0\chi^{(2)}_{ijk}(E_j(\omega_2)E^*_k(\omega_1) + E_k(\omega_2)E^*_j(\omega_1))$, where $i \neq j \neq k$ represent the Cartesian coordinates. The AlGaAs crystal is supposed to be tilted by 45° with respect to the [001] axis, corresponding to a (110)-oriented wafer, where the surface normal is aligned along the [110] crystallographic direction. The DFG efficiency, η, is defined as $\eta = P_{DFG}/(P_{\lambda_1} \cdot P_{\lambda_2})$ where P_{DFG} is the power radiated at THz, while P_{λ_1} and P_{λ_2} are the incident powers

This article has been accepted for publication in IEEE Photonics Journal. This is the author's version which has not been fully edited and content may change prior to final publication. Citation information: DOI 10.1109/JPHOT.2026.3663297

of the two pumps.

Figure 3(a) shows the numerically-computed η, when keeping the normal-incidence excitation wavelength λ_2 fixed at 1452.56 nm ($\omega_2 = 206.39$ THz) and varying both the angle of incidence θ and the wavelength λ_1 of the second source. As θ increases, the MTD excited under oblique incidence follows the same trend reported in Figure 2(d). For example, when $\theta = 1°$, the high-Q toroidal resonance is excited at $\lambda_1 = 1453.87$ nm, corresponding to a frequency $\omega_1 = 206.2$ THz. The associated conversion efficiency, denoted as $\eta_{1°}$, reaches its maximum when $\omega_{\text{DFG}} = \omega_2 - \omega_1 = 0.19$ THz, which corresponds to the simultaneous excitation of the MTD at both source frequencies.

Figure 3(b) reports the amplitude of the AlGaAs $\chi^{(2)}$ coefficient in the 0–9 THz range, i.e., the considered emission band. In the THz regime the second order nonlinear susceptibility of AlGaAs is modeled by using the Faust Henry approach, which sums a constant electronic term and Lorentz oscillators representing transverse optical phonon resonances. The phonon terms cause peaks in the $|\chi^{(2)}|$ spectrum where the denominator of each Lorentz term approaches zero, corresponding to enhanced ionic contribution near lattice resonances. These peaks physically signify that lattice vibrations strongly boost the nonlinear response compared to the non resonant electronic background. The model parameters are obtained from [16]. The resulting dispersion shows pronounced enhancement of $\chi^{(2)}$ around the transverse optical phonon frequencies, which are important for THz generation processes. From 3(b) it can be observed that the $|\chi^{(2)}|$ amplitude is relatively small in the low-THz region, showing a dip around 1.9 THz and a pronounced peak reaching 10^4 pm/V near 8 THz. Since the nonlinear THz field generation depends on both the resonances of the two interacting modes and the amplitude of $\chi^{(2)}$, an increasing frequency separation between the two pump sources (up to 8 THz) allows the process to benefit from the additional enhancement provided by the large nonlinear susceptibility. Figure 3(a) clearly illustrates this trend: each curve corresponds to a specific angle of incidence and shows the conversion efficiency η as a function of λ_1. The efficiency peak always occurs at the frequencies that excite the MTD at the pump wavelengths; however, the overall behavior is also mediated by the $\chi^{(2)}$ amplitude. In particular, the $\eta_{3°}$ curve is negatively affected by the dip in $\chi^{(2)}$, whereas the $\eta_{7.6°}$ curve represents the optimal case, where the two MTD resonances are excited at frequencies whose difference corresponds to the maximum value of $\chi^{(2)}$. In particular, when $\theta = 7.6°$, the efficiency $\eta_{7.6°}$ reaches a record value of $5 \cdot 10^{-2}$ W^{-1} around 8 THz, exceeding by nine orders of magnitude the efficiency of an AlGaAs slab excited under the same conditions. All additional nonlinear optical effects capable of inducing saturation are omitted from the present model and comparison. For completeness, let us recall that in dielectric nanoantennas, when exciting near the magnetic dipole resonance, the absolute THz generation efficiency has been estimated to be on the order of $\approx 10^{-7}$ W^{-1}, representing an enhancement of approximately eight orders of magnitude compared to state-of-the-art plasmonic split-ring resonators [16]. Additionally, dielectric metasurfaces supporting magnetic and electric resonances with relatively low Q-factors have been experimentally shown to enhance THz emission by up to a factor of ≈40 relative to the bare substrate [18]. These results highlight the importance of using dielectric materials to maximize the interaction volume, as well as the critical role of the involved modes in confining the field to further boost efficiency.

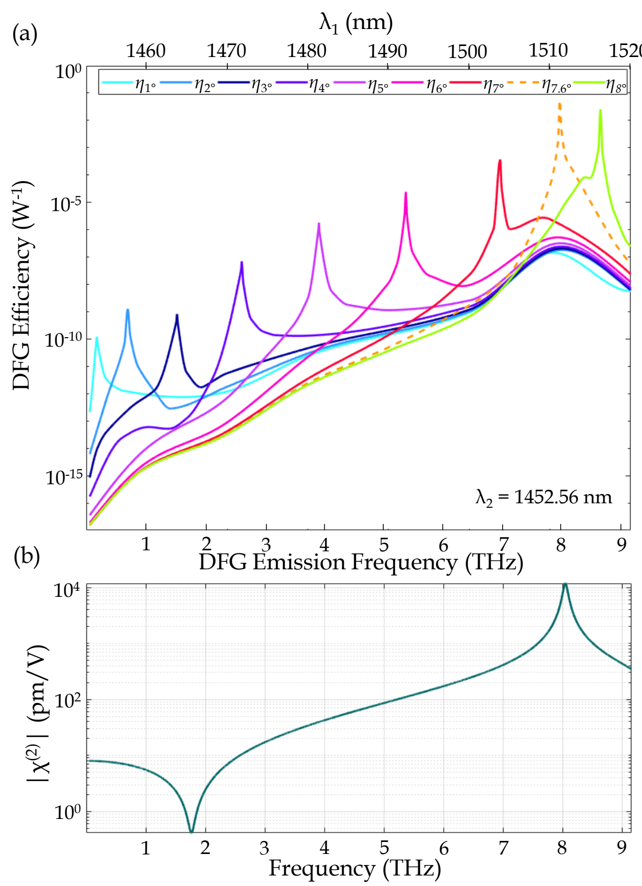

Fig. 3. (a) DFG efficiency obtained by fixing the wavelength λ_2 of the normally incident pump and varying the angle of incidence θ of the oblique pump, shown as a function of the corresponding nonlinear emission frequency ω_{DFG}. Each curve, labeled as $\eta_{1°}$, $\eta_{2°}$, and so on, corresponds to a specific incidence angle. The upper horizontal axis indicates the wavelength λ_1. (b) Amplitude of the AlGaAs nonlinear susceptibility, $|\chi^{(2)}|$, as a function of frequency.

To systematically quantify this enhancement, we introduce the Relative DFG Efficiency (RDE), defined as the ratio between the DFG peak efficiency of the metasurface and that of the unstructured AlGaAs slab, having the same thickness as the proposed structure. Figure 4(a) shows the RDE as a function of L for the configuration considered so far, in which the radiation at λ_1 impinges at $\theta = 8°$ while that at λ_2 is normally incident on the metasurface, thus enabling a direct comparison of the performance enhancement achieved through the metasurface design. Since the excitation wavelength of the MTD resonances shifts slightly for different values of L, the comparison is performed by tracking the modes and evaluating the response at the exact resonance wavelengths corresponding to the high-Q resonances. As one might expect, the RDE decreases drastically with increasing L, that is, as the

Q-factor of the MTD excited at the fundamental frequencies decreases. Figures 4(b) and (c) illustrate the corresponding magnetic field distributions for an oblique incidence of $8°$ and the nonlinear DFG electric field at $L = 10$ nm and $L = 60$ nm, respectively. It can be observed that for $L = 10$ nm, the magnetic field vectors form two opposite circular distributions in the xy plane. This configuration clearly evidences the excitation of a MTD mode, characterized by strong magnetic confinement, indicative of a high-quality resonance. Conversely, for $L = 60$ nm [Figure 4(c)], the magnetic field pattern becomes significantly weaker, indicating that the magnetic loops are partially disrupted. The deterioration of this well-arranged magnetic field is associated with the reduction of the MTD Q-factor and, consequently, a lower overlap between the interacting fields. As a result, the metasurface efficiency and the associated DFG response decrease notably in this regime. In any case, Fig. 4 provides clear evidence of the potential offered by the proposed device. From an experimental perspective, fabrication tolerances are expected to mainly affect the resonance linewidth and the associated Q-factor; nevertheless, MTD modes are known to be robust against moderate geometrical variations that are well within the capabilities of standard electron-beam lithography and dry-etching processes for dielectric metasurfaces, as experimentally shown in [33]. Recent experimental advances have demonstrated that ultrahigh-Q resonances in dielectric metasurfaces are not only theoretically accessible but also practically realizable through robust design strategies. In particular, tetramer metasurfaces exploiting centroid symmetry protection and area-conservation principles have been experimentally shown to support high-Q factors modes exceeding 10^4, while maintaining fabrication tolerance and stability over a wide parameter space [46]. Related works have further reported low-index-contrast dielectric metasurfaces sustaining quasi-BIC resonances with Q-factors approaching or exceeding 10^5 [47], emphasizing that extremely narrow resonances can be achieved without requiring prohibitively fine geometrical features or extreme material parameters. Furthermore, quasi-BIC-based metasurfaces have been experimentally realized to enhance emission processes and light–matter interactions [48], demonstrating scalability and compatibility with standard nanofabrication techniques. Collectively, these studies confirm that qBIC resonances can be engineered in realistic dielectric platforms with experimentally accessible geometries. Moreover, the proposed excitation scheme requires angular alignment within only a few degrees, which can be readily achieved using conventional free-space optical setups equipped with precision rotation stages. These considerations suggest that the predicted performance could be realistically achieved in future experiments by combining angle-resolved linear spectroscopy with continuous-wave or narrowband near-infrared pump lasers, while the generated THz emission may be detected via electro-optic sampling, as commonly adopted in metasurface-based DFG experiments [49].

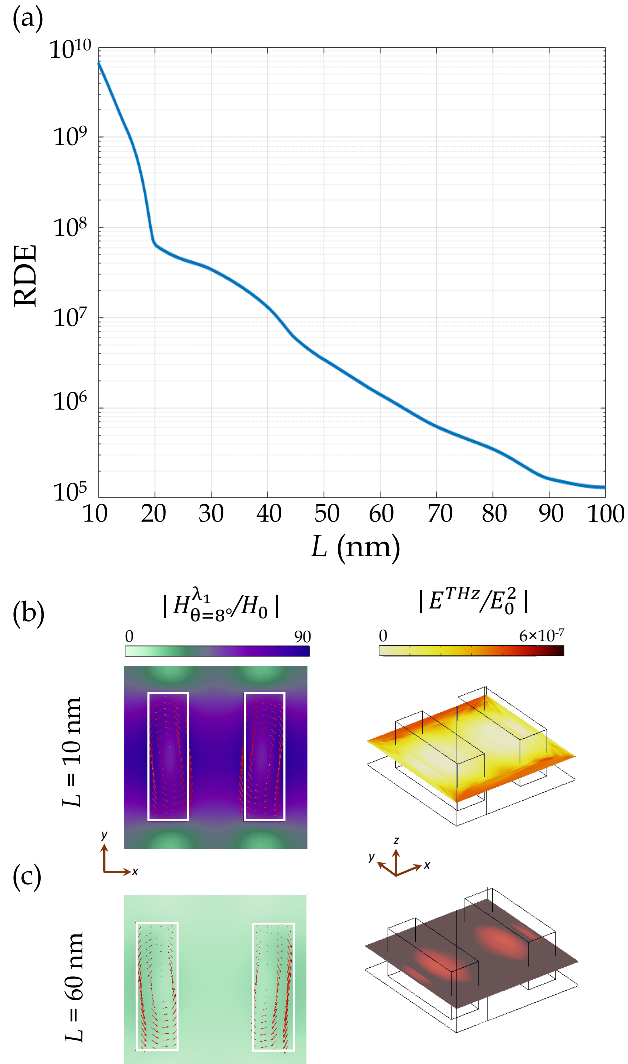

Fig. 4. (a) The Relative DFG Efficiency, RDE, as a function of L. (b) Left: magnetic field distribution when $\theta = 8°$. Right: THz Electric field distribution. $L = 10$ nm (c) Same as (b) for $L = 60$ nm. E_0 and H_0 represent the incident electric and magnetic field amplitude, respectively.

III. Conclusions

In summary, we have theoretically demonstrated highly efficient THz emission via DFG in a properly designed AlGaAs dielectric metasurface that supports two distinct high-Q MTD resonances at the NIR pump frequencies, namely ω_1 and ω_2. The simultaneous excitation of these MTD modes—one at normal incidence (ω_2) and the other at a small oblique angle (ω_1)—enables strong field confinement. Specifically, we tune the incidence angle of the ω_1 resonance to shift its frequency position in order to reach a frequency difference with respect to ω_2 up to $\omega_{DFG} = \omega_2 - \omega_1 = 8$ THz. In this way, the DFG emission can be nonlinearly generated by harnessing both the large Q-factor of the NIR resonances and the peak of the AlGaAs $\chi^{(2)}$ nonlinearity actually occurring near ω_{DFG}. This results in a THz generation efficiency exceeding that of an unstructured slab by more than nine orders of magnitude. Moreover, the structure exhibits a relatively broad angular acceptance, which in principle allows excitation with a numerical aperture exceeding 0.13. In addition, the dispersive nature and energy confinement associated with the excited qBIC mode could potentially relax the lateral size requirements for the metasurface to operate as an effectively infinite structure.

These findings highlight the potential of semiconductor-based metasurfaces as compact, CMOS-compatible platforms for efficient, tunable, and integrable THz sources, and provide valuable design guidelines for future nonlinear photonic and optoelectronic devices leveraging multipolar and toroidal resonances.

IV. Computational Methodology

In this section, we provide a comprehensive description of the simulation framework, including all relevant parameters, to ensure full reproducibility. As outlined above, the numerical procedure is organized into three sequential stages. In the first two stages, the linear electromagnetic response at the pump frequencies is computed using a scattering-field approach. The substrate is modeled with a refractive index of 1.46, while the complex refractive index of AlGaAs is described using the Forouhi-Bloomer dispersion relations, which provide the permittivity across the entire frequency range considered, as demonstrated in [16]. For the computation of the scattered power of the multipoles shown in Fig. 2(a), we adopt the definitions of the main Cartesian multipole moments from [33]. Once the linear solutions are obtained, and the local electric fields within the structure are known, the nonlinear polarization sources are constructed. In the final stage, a full-wave simulation is performed at the generated frequency, where the nonlinear currents driving the emitted radiation are calculated as already shown in [16], [18]. To simulate the DFG process in Comsol, knowledge of the AlGaAs THz nonlinear susceptibility is required; therefore, the Faust-Henry model is employed, incorporating both electronic and ionic contributions, using the same approach reported in [16]. This methodology ensures numerical stability and establishes a direct, transparent connection between the linear resonant response and the resulting nonlinear emission.

References

[1] W. Yang et al., "All-dielectric metasurface for high-performance structural color," *Nat. Commun.*, vol. 11, no. 1, p. 1864, Apr. 2020. DOI: 10.1038/s41467-020-15773-0.

[2] Y. Yang et al., "Multimode directionality in all-dielectric metasurfaces," *Phys. Rev. B*, vol. 95, no. 16, p. 165 426, Apr. 2017. DOI: 10.1103/PhysRevB.95.165426.

[3] A. Leitis et al., "All-dielectric programmable huygens' metasurfaces," *Adv. Funct. Mater.*, vol. 30, no. 19, p. 1 910 259, Mar. 2020. DOI: 10.1002/adfm.201910259.

[4] S. Jahani and Z. Jacob, "All-dielectric metamaterials," *Nat. Nanotechnol.*, vol. 11, no. 1, pp. 23–36, Jan. 2016. DOI: 10.1038/nnano.2015.304.

[5] I. Allayarov, A. B. Evlyukhin, and A. Calà Lesina, "Multiresonant all-dielectric metasurfaces based on high-order multipole coupling in the visible," *Opt. Express*, vol. 32, no. 4, pp. 5641–5658, Feb. 2024. DOI: 10.1364/OE.511172.

[6] V. E. Babicheva and A. B. Evlyukhin, "Mie-resonant metaphotonics," *Adv. Opt. Photonics*, vol. 16, no. 3, pp. 539–658, Aug. 2024. DOI: 10.1364/AOP.510826.

[7] R. C. Devlin, M. Khorasaninejad, W. T. Chen, J. Oh, and F. Capasso, "Broadband high-efficiency dielectric metasurfaces for the visible spectrum," *Proc. Natl. Acad. Sci. USA*, vol. 113, no. 38, pp. 10 473–10 478, Jul. 2016. DOI: 10.1073/pnas.1611740113.

[8] M. Li, Y. Liu, Y. Wu, L. Ma, and Z. Duan, "High-responsivity dielectric metasurface si-based ingaas photodetector," *Opt. Lett.*, vol. 50, no. 17, pp. 5526–5529, Aug. 2025. DOI: 10.1364/OL.571713.

[9] V. F. Gili et al., "Monolithic algaas second-harmonic nanoantennas," *Opt. Express*, vol. 24, no. 14, pp. 15 965–15 971, Jul. 2016. DOI: 10.1364/OE.24.015965.

[10] J. Y. Lee et al., "Cmos-compatible si metasurface at visible wavelengths prepared by low-temperature green laser annealing," *Nanotechnol.*, vol. 30, no. 4, p. 045 301, Nov. 2018. DOI: 10.1088/1361-6528/aaecbd.

[11] E. Mikheeva et al., "Cmos-compatible all-dielectric metalens for improving pixel photodetector arrays," *APL Photonics*, vol. 5, no. 11, Oct. 2020. DOI: 10.1063/5.0022162.

[12] M. Movsisyan, A. A. Al-Rossais, S. Sayeed, and G. Movsisyan, "Applications of terahertz waves in medical diagnostics: A literature review," *Int. J. Community Med. Public Health*, vol. 11, no. 6, p. 2450, May 2024. DOI: 10.18203/2394-6040.ijcmph20241512.

[13] R. Li, C. Li, H. Li, S. Wu, and G. Fang, "Study of automatic detection of concealed targets in passive terahertz images for intelligent security screening," *IEEE Trans. Terahertz Sci. Technol.*, vol. 9, no. 2, pp. 165–176, Dec. 2018. DOI: 10.1109/TTHZ.2018.2889407.

[14] T. Nagatsuma et al., "Terahertz wireless communications based on photonics technologies," *Opt. Express*, vol. 21, no. 20, pp. 23 736–23 747, Sep. 2013. DOI: 10.1364/OE.21.023736.

[15] Z. Chen et al., "Terahertz wireless communications for 2030 and beyond: A cutting-edge frontier," *IEEE Commun. Mag.*, vol. 59, no. 11, pp. 66–72, Dec. 2021. DOI: 10.1109/MCOM.011.2100195.

[16] U. A. Leon et al., "Thz-photonics transceivers by all-dielectric phonon-polariton nonlinear nanoantennas," *Sci. Rep.*, vol. 12, no. 1, p. 4590, Mar. 2022. DOI: 10.1038/s41598-022-08695-y.

[17] F. Habibighahfarokhi et al., "Nonlinear dielectric metasurfaces for terahertz applications," in *Photonics*, MDPI, vol. 12, Apr. 2025, p. 370. DOI: 10.3390/photonics12040370.

[18] L. Peters et al., "Resonant fully dielectric metasurfaces for ultrafast terahertz pulse generation," *Adv. Opt. Mater.*, vol. 12, no. 16, p. 2 303 148, Apr. 2024. DOI: 10.1002/adom.202303148.

[19] J. Jeong et al., "High quality factor toroidal resonances in dielectric metasurfaces," *ACS Photonics*, vol. 7, no. 7, pp. 1699–1707, Jun. 2020. DOI: 10.1021/acsphotonics.0c00179.

[20] S. Xu et al., "Experimental observation of toroidal dipole modes in all-dielectric metasurfaces," *Adv. Opt.

Mater., vol. 7, no. 4, p. 1 801 166, Dec. 2019. DOI: 10.1002/adom.201801166.

[21] Y. Wang, Z. Han, Y. Du, and J. Qin, "Ultrasensitive terahertz sensing with high-q toroidal dipole resonance governed by bound states in the continuum in all-dielectric metasurface," *Nanophotonics*, vol. 10, no. 4, pp. 1295–1307, Jan. 2021. DOI: 10.1515/nanoph-2020-0582.

[22] A. E. Miroshnichenko et al., "Nonradiating anapole modes in dielectric nanoparticles," *Nat. Commun.*, vol. 6, no. 1, p. 8069, Aug. 2015. DOI: 10.1038/ncomms9069.

[23] L. Wei, Z. Xi, N. Bhattacharya, and H. P. Urbach, "Excitation of the radiationless anapole mode," *Optica*, vol. 3, no. 8, pp. 799–802, Jul. 2016. DOI: 10.1364/OPTICA.3.000799.

[24] T. Kaelberer, V. Fedotov, N. Papasimakis, D. Tsai, and N. Zheludev, "Toroidal dipolar response in a metamaterial," *Science*, vol. 330, no. 6010, pp. 1510–1512, Nov. 2010. DOI: 10.1126/science.1197172.

[25] Y. He, G. Guo, T. Feng, Y. Xu, and A. E. Miroshnichenko, "Toroidal dipole bound states in the continuum," *Phys. Rev. B*, vol. 98, no. 16, p. 161 112, Oct. 2018. DOI: 10.1103/PhysRevB.98.161112.

[26] V. Savinov, V. Fedotov, and N. I. Zheludev, "Toroidal dipolar excitation and macroscopic electromagnetic properties of metamaterials," *Phys. Rev. B*, vol. 89, no. 20, p. 205 112, May 2014. DOI: 10.1103/PhysRevB.89.205112.

[27] C. Zhou, S. Li, Y. Wang, and M. Zhan, "Multiple toroidal dipole fano resonances of asymmetric dielectric nanohole arrays," *Phys. Rev. B*, vol. 100, no. 19, p. 195 306, Nov. 2019. DOI: 10.1103/PhysRevB.100.195306.

[28] S. You, Y. Zhang, M. Fan, S. Luo, and C. Zhou, "Strong light–matter interactions of exciton in bulk ws2 and a toroidal dipole resonance," *Opt. Lett.*, vol. 48, no. 6, pp. 1530–1533, Mar. 2023. DOI: 10.1364/OL.481063.

[29] J. Lv et al., "Optical anapole modes in gallium phosphide nanodisk with forked slits for electric field enhancement," *Nanomaterials*, vol. 11, no. 6, p. 1490, Jun. 2021. DOI: 10.3390/nano11061490.

[30] R. Masoudian Saadabad, M. Cai, F. Deng, L. Xu, and A. E. Miroshnichenko, "Structured light excitation of toroidal dipoles in dielectric nanodisks," *Phys. Rev. B*, vol. 104, no. 16, p. 165 402, Oct. 2021. DOI: 10.1103/physrevb.104.165402.

[31] R. Xu and J. Takahara, "Hollow mie resonators based on toroidal magnetic dipole mode with enhanced sensitivity in refractometric sensing," *Appl. Phys. Express*, vol. 17, no. 1, p. 012 005, Jan. 2024. DOI: 10.35848/1882-0786/ad197e.

[32] X. Wang et al., "Tuning the magnetic toroidal dipole response in dielectric metasurfaces," *J. Opt. Soc. Am. B*, vol. 40, no. 3, pp. 560–566, Feb. 2023. DOI: 10.1364/JOSAB.481376.

[33] Y. Zhang et al., "High-q magnetic toroidal dipole resonance in all-dielectric metasurfaces," *APL Photonics*, vol. 9, no. 7, Jul. 2024. DOI: 10.1063/5.0208936.

[34] N. Li et al., "Ultrasensitive metasurface sensor based on quasi-bound states in the continuum," *Nanophotonics*, vol. 14, no. 4, pp. 485–494, Feb. 2025. DOI: 10.1515/nanoph-2024-0728.

[35] H. Duan et al., "Efficient second-harmonic generation in a lithium niobate metasurface governed by high-q magnetic toroidal dipole resonances," *Opt. Lett.*, vol. 49, no. 19, pp. 5539–5542, Sep. 2024. DOI: 10.1364/OL.533402.

[36] H. Duan et al., "Nonlinear chiroptical response in lithium niobate metasurface driven by quasi-bound states in the continuum," *Appl. Phys. Lett.*, vol. 125, no. 21, Nov. 2024. DOI: 10.1063/5.0242454.

[37] S. Feng, T. Liu, W. Chen, F. Wu, and S. Xiao, "Enhanced sum-frequency generation from etchless lithium niobate empowered by dual quasi-bound states in the continuum," *Sci. China-Phys. Mech. Astron.*, vol. 66, no. 12, p. 124 214, Nov. 2023. DOI: 10.1007/s11433-023-2223-5.

[38] T. Liu, M. Qin, F. Wu, and S. Xiao, "High-efficiency optical frequency mixing in an all-dielectric metasurface enabled by multiple bound states in the continuum," *Phys. Rev. B*, vol. 107, no. 7, p. 075 441, Feb. 2023. DOI: 10.1103/PhysRevB.107.075441.

[39] M. Qin, F. Wu, T. Liu, D. Zhang, and S. Xiao, "Enhanced third-harmonic generation and degenerate four-wave mixing in an all-dielectric metasurface via brillouin zone folding induced bound states in the continuum," *Phys. Rev. B*, vol. 111, no. 3, p. 035 414, Jan. 2025. DOI: 10.1103/PhysRevB.111.035414.

[40] L. Xu et al., "Enhanced four-wave mixing from multi-resonant silicon dimer-hole membrane metasurfaces," *New J. Phys.*, vol. 24, no. 3, p. 035 002, Mar. 2022. DOI: 10.1088/1367-2630/ac55b2.

[41] G. Sanderson et al., "Infrared imaging with nonlinear silicon resonator governed by high-q quasi-bic states," *J. Opt.*, vol. 26, no. 6, p. 065 505, May 2024. DOI: 10.1088/2040-8986/ad44a9.

[42] Z. Zheng et al., "Broadband infrared imaging governed by guided-mode resonance in dielectric metasurfaces," *Light Sci. Appl.*, vol. 13, no. 1, p. 249, Sep. 2024. DOI: 10.1038/s41377-024-01535-w.

[43] A. Theodosi et al., "Graphene nanosheet-gold nanopatch metasurfaces for nonlinear response at thz frequencies," *ACS Appl. Nano Mater.*, Dec. 2025. DOI: 10.1021/acsanm.5c04665.

[44] P. Franceschini et al., "Intrapulse multimodal four-wave sum mixing in the visible range from high contrast index grating with pmma layer," *Light Sci. Appl.*, vol. 15, no. 1, p. 51, Jan. 2026. DOI: 10.1038/s41377-025-02090-8.

[45] D. C. Zografopoulos and O. Tsilipakos, "Recent advances in strongly resonant and gradient all-dielectric metasurfaces," *Mater. Adv.*, vol. 4, no. 1, pp. 11–34, Nov. 2023. DOI: 10.1039/D2MA00910B.

[46] C. Zhou, R. Jin, H. He, J. Huang, G. Li, and L. Huang, "Robust ultrahigh-q resonances in tetramer metasurfaces through centroid symmetry protection and area conservation," *Light Sci. Appl.*, vol. 15, no. 1, p. 84, Jan. 2026. DOI: 10.1038/s41377-025-02164-7.

[47] K. Watanabe, T. Nagao, and M. Iwanaga, "Low-contrast bic metasurfaces with quality factors exceeding 100,000," *Nano Lett.*, vol. 25, no. 7, pp. 2777–2784, Feb. 2025. DOI: 10.1021/acs.nanolett.4c05880.

[48] J. Guo et al., "Topologically engineered high-q quasi-bic metasurfaces for enhanced near-infrared emission in pbs quantum dots," *Nano Lett.*, vol. 25, no. 6, pp. 2357–2365, Jan. 2025. DOI: 10.1021/acs.nanolett.4c05710.

[49] S. Sideris, H. Zixian, C. McDonnell, G. Li, and T. Ellenbogen, "Holographic thz beam generation by nonlinear plasmonic metasurface emitters," *ACS photonics*, vol. 10, no. 8, pp. 2972–2979, Aug. 2023. DOI: 10.1021/acsphotonics.3c00775.